Langmuir

Article

pubs.acs.org/Langmuir

Succinimidyl Ester Surface Chemistry: Implications of the Competition between Aminolysis and Hydrolysis on Covalent Protein Immobilization

China Y. Lim,[†] Nicholas A. Owens,[‡] Ronald D. Wampler,[⊥] Yixin Ying,[‡] Jennifer H. Granger,[⊥] and Marc D. Porter*[,†,‡,§,∥,⊥]

[†]Departments of Chemical Engineering, [‡]Chemistry, [§]Bioengineering, and [∥]Pathology and the [⊥]Nano Institute of Utah, University of Utah, Salt Lake City, Utah 84112, United States

Makoto Takahashi and Katsuaki Shimazu

Division of Environmental Materials Science, Graduate School of Environmental Science and Section of Materials Science, Faculty of Environmental Earth Science, Hokkaido University, Sapporo 060-0810, Japan

ABSTRACT: *N*-Hydroxysuccinimide (NHS) ester terminal groups are commonly used to covalently couple amine-containing biomolecules (e.g., proteins and peptides) to surfaces via amide linkages. This one-step aminolysis is often performed in buffered aqueous solutions near physiological pH (pH 6 to pH 9). Under these conditions, the hydrolysis of the ester group competes with the amidization process, potentially degrading the efficiency of the coupling chemistry. The work herein examines the efficiency of covalent protein immobilization in borate buffer (50 mM, pH 8.50) using the thiolate monolayer formed by the chemisorption of dithiobis (succinimidyl propionate) (DSP) on gold films. The structure and reactivity of these adlayers are assessed via infrared spectroscopy (IR), X-ray photoelectron spectroscopy (XPS), electrochemical reductive desorption, and contact angle measurements. The hydrolysis of the DSP-based monolayer is proposed to follow a reaction mechanism with an initial nucleation step, in contrast to a simple pseudo first-order reaction rate law for the entire reaction, indicating a strong dependence of the interfacial reaction on the packing and presence of defects in the adlayer. This interpretation is used in the subsequent analysis of IR-ERS kinetic plots which give a heterogeneous aminolysis rate constant, k_a, that is over 3 orders of magnitude lower than that of the heterogeneous hydrolysis rate constant, k_h. More importantly, a projection of these heterogeneous kinetic rates to protein immobilization suggests that under coupling conditions in which low protein concentrations and buffers of near physiological pH are used, proteins are more likely physically adsorbed rather than covalently linked. This result is paramount for biosensors that use NHS chemistry for protein immobilization due to effects that may arise from noncovalently linked proteins.

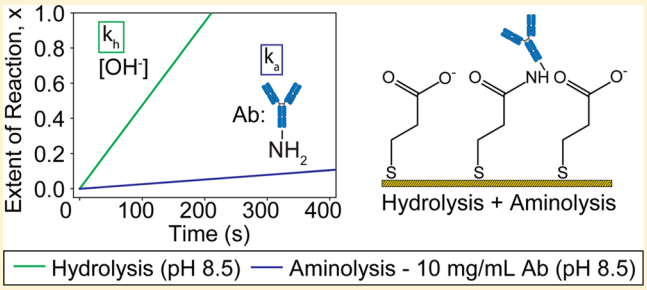

INTRODUCTION

N-Hydroxysuccinimide (NHS) and other activated esters are often used as coupling agents to covalently tether antibodies, enzymes, peptides, and other biomaterials to surfaces for use in bioanalytical sensors.[1−3] There are two common strategies for fabricating NHS-functionalized surfaces: (1) reaction of surface carboxylate groups with NHS and *N*-ethyl-*N*-(3-dimethylamino)propyl carbodiimide (EDAC)[4] and (2) direct derivatization of gold, silicon, and other surfaces with an NHS-containing coating.[5] In both cases, coupling is achieved by treating the NHS-activated surface with a solution of a primary amine-containing reactant. This step (i.e., aminolysis) forms amide linkages with the sterically accessible amines of the reactant.

We have used this methodology to construct antibody-modified surfaces for the selective capture and labeling of markers in immunoassays for the detection of infectious diseases, cancer, and nutrient deficiencies.[6,7] Scheme 1 summarizes our two-step procedure. Step 1 forms the active ester surface by immersion of a gold substrate in a 0.10 mM solution of 3,3′-dithiobis (succinimidyl) propionate (DSP), i.e., Lomant's reagent, in ethanol.[8] This step chemisorbs a monolayer of the gold-bound thiolate of DSP, 3-*N*-hydroxysuccinimidyl propanethiolate.[9] Step 2 reacts the NHS-activated substrate in a buffered, protein-containing solution. We typically carry out this step in borate buffer (pH 8.50, 50 mM), which, as recently reviewed,[3] is similar to the conditions commonly recommended for this reaction. This step is

Received: August 27, 2014
Published: October 15, 2014

Scheme 1. Method for Covalent Coupling of Capture Antibody Layer in Immunoassay Using an NHS Terminated Monolayer and Primary Amines in Antibodies[a]

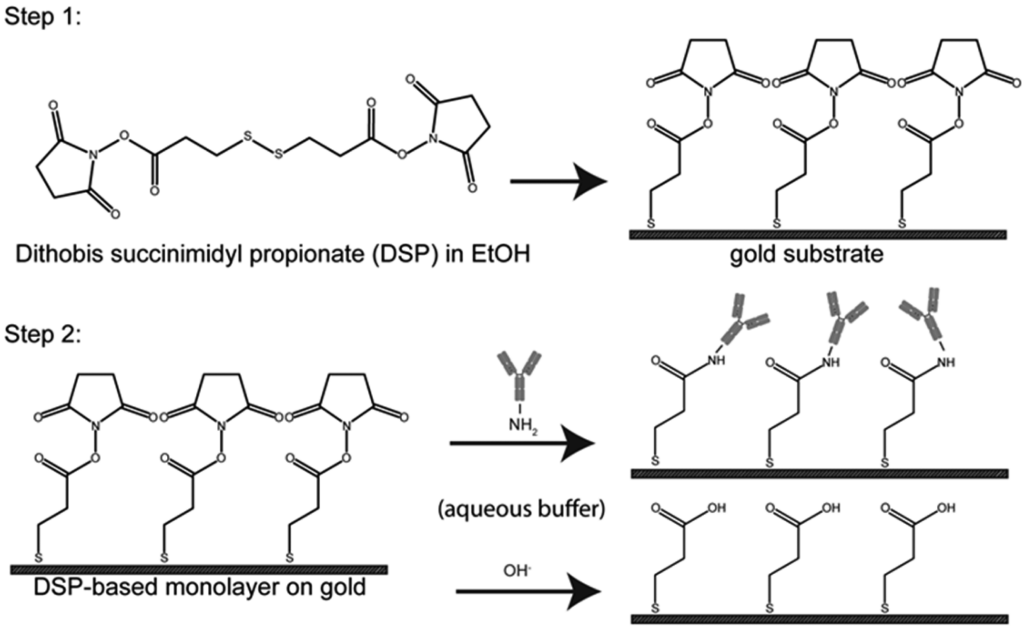

[a]Step 1 forms the NHS-terminated monolayer on gold by chemisorption of DSP. Step 2 reacts the NHS-terminated monolayer on gold with an antibody in aqueous buffer (aminolysis); the competing reaction with hydroxide ions (hydrolysis) is shown in parallel.

designed to immobilize proteins on the surface via an amide linkage.

Along with steric effects,[10] there are two more factors to consider when using aminolysis for surface immobilization. First, the amine groups of the biological reactant act as nucleophiles, viz. deprotonated amines.[11] Thus, the pH of the coupling solution controls the nucleophile concentration. Second, the coupling conditions should not alter the inherent reactivity of the biomolecule (e.g., the binding affinity of an antibody to an antigen). As such, these reactions are typically carried out in an aqueous solution at a pH and ionic strength close to those found physiologically (e.g., pH ∼6−9 and 150 mM NaCl) in order to preserve the tertiary structure of proteins.[12,13] This issue is central in the immobilization of antibodies in that structural denaturation may reduce the affinity for antigen binding.[10] The use of physiological reaction conditions, however, can induce the hydrolysis of the activated ester group, which would reduce the number of reactive sites for aminolytic coupling and decrease the efficiency of the linking chemistry.[3,14] Thus, the coupling conditions must strike a balance between the rates of the two reactions, aminolysis and hydrolysis, both of which are affected by pH, buffer composition, reactant concentration, temperature, and other factors.[1,3]

There is a large body of evidence, including that from our laboratory,[15] which supports the effectiveness of step 2 in Scheme 1. Much of this evidence is based on measurements of the biological or chemical activity of the immobilized species. Examples include the colorimetric[16,17] and electrochemical detection[18] of the activity of an immobilized enzyme or a tethered redox molecule. More so, infrared external reflection spectroscopy (IR-ERS)[19] and X-ray photoelectron spectroscopy (XPS)[20] have been used in efforts to detect the formation of an amide linkage after protein immobilization. However, while supporting the presence of a protein layer, a clear interpretation of these measurements is compromised by the difficulty in identifying the presence of the aminolytically formed amide linkage vis-à-vis the large number of amide groups inherent in the protein itself.[21] As a consequence, studies have used monoamines (e.g., lysine[22] and butylamine[23]) as reactive mimics to simplify the spectroscopic analysis and, by inference, assess the effectiveness of the aminolysis reaction when using proteins. Nonetheless, the extension of these results to an exacting determination of protein tethering is subject to the inability to rule out the presence of proteins due to nonspecific adsorption.[24]

This paper reports on the results of an investigation of the effectiveness of step 2 in Scheme 1 by an examination of the competitive rates of interfacial aminolysis and base hydrolysis reactions of the DSP-based monolayer on gold substrates. The heterogeneous base hydrolysis reaction rate was examined using borate buffer (pH 8.50, 50 mM). The rate of aminolysis measured in the same buffer system used ethylamine as a mimic of the reactivity with respect to protein immobilization. These findings are presented and discussed after we describe the results of characterization of the DSP-based monolayer on gold by IR-ERS, XPS, electrochemical techniques, and contact angle measurements. Ultimately, these data are used to estimate the effectiveness of the aminolytic coupling reaction in Scheme 1 as it applies to immobilizing proteins on a biosensor surface.

EXPERIMENTAL SECTION

Reagents. Dithiobis (succinimidyl propionate) (DSP, >95%), ethylamine hydrochloride, 1,4-dioxane, and borate buffer (50 mM, pH 8.50) were obtained from Fisher Scientific; 200 proof ethanol from AAPER Pharmaco; potassium bromide (KBr, 99+%, IR grade) and tetramethylammonium chloride (TMAC, >98%) from Acros Organics; *N*-(benzoyloxy) succinimide (NBS) and gold shot (99.995%) from Alfa Aesar; and 1-octadecane-d_{37}-thiol from C/D/N Isotopes. 1,4-Dioxane was dried over molecular sieves (EMD) prior to use. All other chemicals were used as received. Aqueous solutions were prepared

dx.doi.org/10.1021/la503439g | *Langmuir* 2014, 30, 12868−12878

using water purified by passage through a Barnstead water polishing system to obtain water at a resistivity of 18.2 MΩ.

Monolayer Preparation. Substrates used to prepare the DSP-based monolayers were formed on glass slides (25 × 75 mm). The glass slides were first cleaned by immersion in piranha etch [3:1 H_2SO_4:H_2O_2 (30%)] for 10 min, followed by rinsing with copious amounts of high purity water, and subsequently drying under a stream of nitrogen. Caution: Piranha etch reacts violently with most organic materials and must be used and handled with extreme care. The glass slides were then coated by the vapor deposition of a 20 nm chromium adhesion layer and a 200 nm gold film. The gold substrates were then immersed in a 0.10 mM ethanolic solution of DSP. After 16 h, the slides were rinsed with high purity ethanol and dried under a stream of nitrogen.

Infrared Spectroscopy (IRS). IR spectra were obtained using a Nicolet Magna 850 Fourier transform infrared spectrometer equipped with a liquid-nitrogen-cooled mercury cadmium telluride detector. Spectra were collected in a nitrogen atmosphere by coadding 512 scans at a resolution of 4 cm^{-1}. Transmission spectra for powdered samples were taken after dispersion in high purity KBr pellets. External reflection spectra (IR-ERS) used *p*-polarized light incident at 82° from the surface normal and are reported as $-\log R/R_o$, where R is the spectrum of the sample and R_o is that of an octadecanethiolate-d_{37} reference monolayer on gold.

X-ray Photoelectron Spectroscopy (XPS). XPS measurements used a Kratos Axis Ultra DLD XPS with a monochromatic Al X-ray source at an incidence angle of 60°. Spectra were obtained with a 700 × 300 μm hybrid slot size, 12 mA emission current, and 15 kV anode potential; the instrument pressure ranged from 10^{-9} to 10^{-10} Torr. Survey scans were collected at a 160 eV pass energy and 1 eV step size. High resolution scans used a 40 eV pass energy and 0.1 eV step size, with a dwell time of 300 ms in the C(1s) and O(1s) spectral regions and 1.2 s in the N(1s) and S(2p) spectral regions. All binding energies are reported with respect to the Au($4f_{7/5}$) emission band at 84.0 eV.[25] Band shapes were modeled using Gaussian-Lorentzian profiles and a linear or Shirley background subtraction.[26] For spectral deconvolution, fits in O(1s), C(1s), and N(1s) regions were constrained only for band shape; the fits were set to find the minimum number of bands that gave an overall residual of less than 3%. The S(2p) bands were constrained to full widths at half-maximum of 0.9 to 1.3 eV, an integrated S($2p_{1/2}$) band intensity twice that of the S($2p_{3/2}$) band, and separation between the two bands of 1.2 eV.[27]

Electrochemistry. Electrochemical measurements used a three-electrode cell with the gold substrates as the working electrode, platinized platinum foil as the auxiliary electrode, and Ag/AgCl (sat'd KCl) as the reference electrode; all potentials are reported against this electrode. The geometric area of the working electrode was 0.65 cm^2 at a roughness factor of 1.40.[28,29] Voltammetric scans were performed in 0.5 M KOH after sparging with argon (~30 min).

UV-vis Spectroscopy. UV-vis measurements were performed with a Cary 5000 UV-VIS-NIR spectrophotometer at room temperature using a 1.00 cm quartz cuvette. Scans were collected between 350 and 220 nm with an integration time of 0.10 s and a spectral bandwidth of 2 nm. Kinetic measurements recorded the solution absorbance at 260 nm at 0.10 s intervals; the first data point was collected ~10 s after solution mixing.

Contact Angle Measurements. Contact angles were measured with a Dataphysics OCA15EC instrument at room temperature. Deionized water was used as the probe liquid. The advancing, θ_a, and receding, θ_r, contact angles were measured by increasing or decreasing the volume of the droplet, respectively.

Adlayer surface concentration by XPS. The surface concentration for sulfur was determined using a previously documented procedure.[30,31] Briefly, the system was modeled as a uniform film with a thickness (τ) determined from signal attenuation. For film thickness calculations, the signal from the Au(4f) bands of an unmodified gold substrate was used as the reference response (I^0_{Au}), with the intensity of the signal gold sample (I_{Au}) given by

$$I_{Au} = I^0_{Au} \exp\left[-\frac{\tau}{L_{Au}}\right] \quad (1)$$

where L_{Au}, the effective attenuation length, was determined using the NIST Standard Reference Database 82 software.[32]

With the calculated film thickness, the elemental concentration of sulfur, N_s, was found from

$$N_S = N_{Au}\frac{I_X}{I_{Au}}\frac{T_{Au}\sigma_{Au}L^Q_{Au}}{T_S\sigma_S L^Q_S}\frac{\exp\left[-\frac{\tau}{L_{Au}}\right]}{1-\exp\left[-\frac{\tau}{L_S}\right]} \quad (2)$$

In eq 2, N_{Au} is the atomic density of gold (19.28 g/cm^3), T_{Au} and T_s are the respective analyzer transmission functions, σ_{Au} and σ_S are the respective photoelectric cross sections, and L^Q_{Au} and L^Q_S are the appropriate effective attenuation lengths. The value of N_S is then used to calculate the surface concentration ($\Gamma_{NHS,XPS}$) as

$$\Gamma_{NHS,XPS} = N_S\tau \quad (3)$$

Interfacial Kinetics. For the studies of hydrolysis kinetics, DSP-based monolayers on gold-coated glass slides were immersed in a large volume (~60 mL) of 50 mM borate buffer (pH 8.50, buffer capacity of 15 mM) for different periods of time at room temperature. At the end of each time period, each slide was thoroughly rinsed with distilled water, dried with nitrogen, and analyzed via IR-ERS; the rinsing and drying steps collectively required ~20 s. It is assumed that this process quenches the reaction in less than 20 s. The slides were then reimmersed in the borate buffer solution until the end of the next time segment and the rinsing, drying, and analysis procedures were repeated. The same procedure and conditions were used for aminolysis, after the addition of 500 mM ethylamine.

RESULTS AND DISCUSSION

This paper presents findings from an investigation of the reactivity (base hydrolysis and aminolysis) of the NHS-terminated monolayer formed by the spontaneous adsorption of DSP on gold. It describes results from (1) characterizations of the as-formed monolayer by IR-ERS, XPS, electrochemistry, and contact angle measurements to establish the architecture of the adlayer and (2) IR-ERS reaction rate studies of the adlayer in borate buffer (pH 8.50) with and without ethylamine to serve as a basis for a comparison of the respective rates of the base hydrolysis and aminolysis of the terminal NHS group of the adlayer. The reaction rate data, which include measurements of the homogeneous base hydrolysis of the adsorbate precursor (DSP) in aqueous base, are then examined within the context of establishing the effectiveness of this pathway to protein tethering.

Characterization of As-Formed Adlayer. The composition and surface concentration of the as-prepared adlayer were characterized via IR-ERS, XPS, and electrochemistry. IR spectra of DSP and NHS dispersed as a powder in a KBr pellet and of the as-formed DSP-based monolayer on gold are shown in Figure 1 between 2000 and 1000 cm^{-1}. Band assignments are listed in Table 1. The spectral features most characteristic of NHS are the symmetric carbonyl stretch (ν_s(C═O)) at 1780 cm^{-1} and the broader, much stronger envelope of asymmetric carbonyl stretches (ν_a(C═O)) between ~1750 and 1675 cm^{-1}; this envelope reflects contributions from hydrogen bonding and other electronic interactions in the solid phase.[22,33] Bands at lower energy (e.g., the asymmetric C−N−C stretch (ν_a(C−N−C)) at 1219 cm^{-1} and the C−O stretch (ν(C−O)) at 1078 cm^{-1}) are additional succinimidyl group identifiers.[22] All of the above bands are present in the spectra for DSP in KBr and the resulting adlayer. Importantly,

dx.doi.org/10.1021/la503439g | Langmuir 2014, 30, 12868−12878

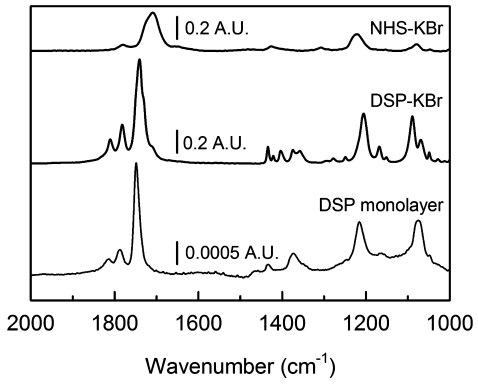

Figure 1. Infrared spectra for NHS and DSP dispersed in KBr and for the DSP-based monolayer chemisorbed on gold.

Table 1. Infrared Spectral Peak Positions and Band Assignments for DSP and NHS Dispersed in KBr and for the DSP-Based Adlayer on Gold[22,33]

		peak position (cm^{-1})		
mode assignment	description	NHS-KBr	DSP-KBr	DSP/Au
ν(C═O)	carbonyl stretch of ester		1814	1820
ν_s(C═O)	symmetric carbonyl stretch of NHS	1780	1788	1787
ν_a(C═O)	asymmetric carbonyl stretch of NHS	1750–1675	1740	1748
δ (CH_2)	methylene scissors deformation	1426	1433	1464
ν_s(C–N–C)	symmetric CNC stretch of NHS	1307	1373	1378
ν_a(C–N–C)	asymmetric CNC stretch of NHS	1219	1216	1215
ν(C–O)	N–C–O of succinimide	1078	1075	1074

the highest energy feature in these two spectra, which is assigned to the carbonyl stretch (ν(C═O)) of the ester linkage between NHS and the alkyl chain of DSP, is expectedly absent in the spectrum for NHS. There are also barely detectable features at much higher energy that correspond to the asymmetric ($\nu_a(CH_2)$) and symmetric ($\nu_a(CH_2)$) stretches of the methylene groups in the alkyl chain at 2922 and 2852 cm^{-1}, respectively (data not shown).[22] There is little evidence (i.e., clear differences between the widths of the two KBr spectra with respect to that for the DSP-based adlayer) of interactions between neighboring NHS groups in the adlayer. These results confirm the presence of the DSP-based adlayer on gold.

The XPS results (spectra a in Figure 2 and Table 2) provide further evidence for the presence of the DSP-derived adlayer. In the O(1s) binding energy region, the two observable bands can be assigned to the C═O (532.1 eV) and C–O (534.4 eV) groups of the NHS terminus.[34] The two bands present in the C(1s) binding energy region at 284.8 and 288.7 eV are assigned to the methylene and carbonyl carbons, respectively.[34,35] The asymmetry in the methylene band is ascribed to the methylene carbon adjacent to the carbonyl carbon.[35] In the S(2p) binding region, there are two bands for the S(2p) couplet: S($2p_{3/2}$) at 161.9 eV and S($2p_{1/2}$) at 163.1 eV. The positions of the two bands in the S(2p) couplet confirm the presence of the gold-bound thiolate formed in the chemisorption of thiols and disulfides on gold.[36] Finally, the N(1s) binding energy region has a single band at 401.6 eV, which is diagnostic of the NHS nitrogen.[20,34] The remaining spectra in Figure 2 are discussed in the next section.

The surface concentration, $\Gamma_{NHS,XPS}$, of the DSP-based monolayer was calculated by using the spectral intensities from the XPS S(2p) region and the procedures accompanying eqs 1-3.[30,31] This analysis gives a value for $\Gamma_{NHS,XPS}$ of 6.44 ± 0.97 × 10^{-10} mol/cm^2 (n = 5). For comparison, an electrochemical determination of Γ_{NHS}, $\Gamma_{NHS,EC}$, was carried out by measuring the charge required for the one-electron reductive desorption of the adlayer in 0.50 M KOH (aq).[28,38–40] A representative linear sweep voltammogram at 0.100 V/s from these measurements is shown in Figure 3. Two large cathodic waves are evident, a sharper feature with a peak-current maximum at −0.82 V and a broader feature at −1.05 V. The presence of multiple waves is consistent with differences in the sorptive strength of the thiolate to different crystallographic binding sites on a polycrystalline gold surface.[41] Using a linear baseline approximation to estimate the contribution of the double layer charging current, integration of the area under the current-potential curves for 7 different samples yields an average desorption charge of 69.7 ± 5.4 μC/cm^2. After accounting for a roughness factor of 1.40,[28,29] this translates to a surface area normalized charge of 49.8 ± 3.9 μC/cm^2 or a $\Gamma_{NHS,EC}$ of 5.16 ± 0.40 × 10^{-10} mol/cm^2. This value agrees well with the roughness factor corrected value for $\Gamma_{NHS,XPS}$ of 5.86 ± 0.88 × 10^{-10} mol/cm^2. These two values differ by less than 15% from those reported by other laboratories.[5,18] Furthermore, both values are lower than that expected for the $(\sqrt{3} \times \sqrt{3})$ R30° adlayer formed by n-alkanethiols on Au(111), which reflects the difference in the packing density of the bulky NHS terminal group.[42,43]

Compositional Analysis of Reacted Adlayers. XPS was used to confirm the identity of the surface-bound reaction products for hydrolysis and aminolysis (spectra b and c in Figure 2 and Table 2). Immersion of the adlayer for ∼16 h in either borate buffer (pH 8.50, 50 mM) or 500 mM ethylamine in the same borate buffer resulted in the following differences in the adlayer. First, the bands associated with the NHS ester (534.4 eV in the O(1s) and 401.6 eV in the N(1s) spectral regions) are no longer detectable after either treatment, indicative of removal of the NHS group. Second, the presence of the aminolysis reaction product is indicated by the appearance of the N(1s) band at 399.5 eV, which is diagnostic of an amide nitrogen.[20,34,37] The two bands in the C(1s) binding energy region, representative of methylene and carbonyl carbons, are still present after each of the treatments, but their relative intensities have changed in accordance with the expected reaction products. Lastly, the strength of the S(2p) bands remains unchanged, confirming the stability of the gold-bound adlayer under the reaction conditions used herein. These results verify the presence of the expected surface reaction products and are supported by the IR-ERS data in the next section.

Adlayer Base Hydrolysis. The rate of the alkaline hydrolysis for the NHS-activated ester monolayer was monitored as a function of immersion time in borate buffer (pH 8.50, 50 mM) by IR-ERS. As shown in Figure 4, the temporal evolution of the spectra is indicative of the progression in the hydrolytic loss of the NHS group. The ν_a(C═O) at 1748 cm^{-1}, for example, decreases in strength by more than 50% in less than 480 s; this feature is virtually undetectable after 14 min. Other spectral features (*e.g.*, N–C–O band at 1074 cm^{-1} and the carboxylate vibration band at

dx.doi.org/10.1021/la503439g | *Langmuir* 2014, 30, 12868–12878

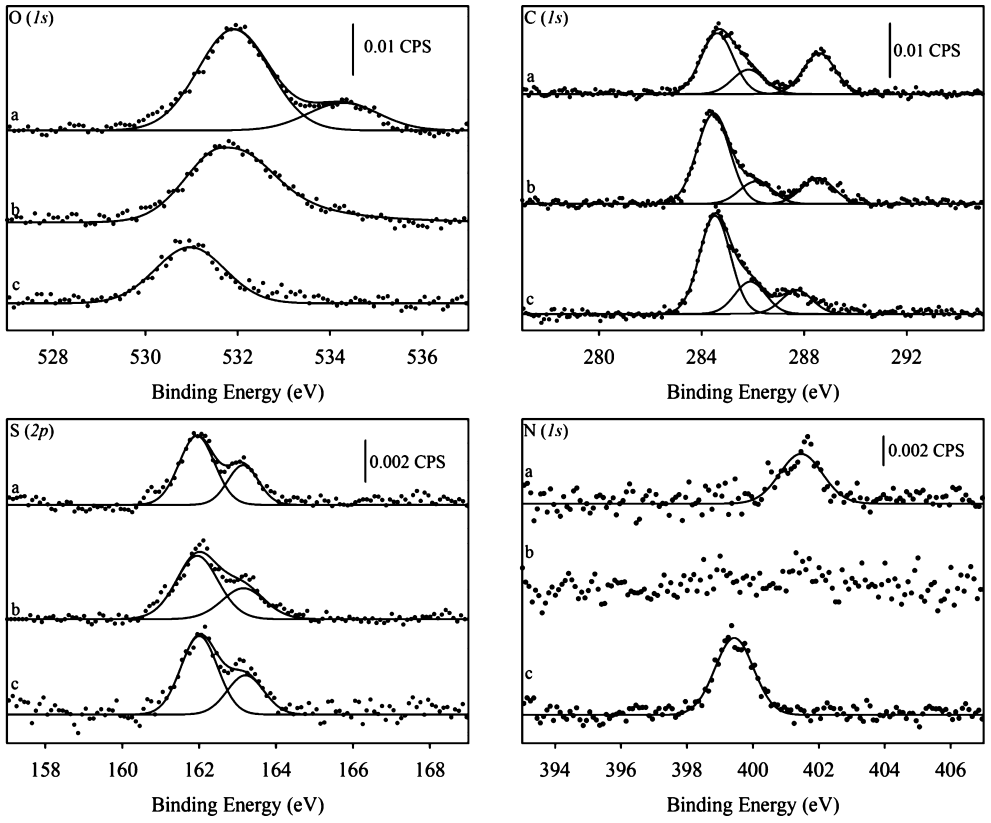

Figure 2. XPS spectra of (a) as-formed DSP-based adlayer on gold, (b) hydrolyzed DSP-based adlayer on gold after overnight (greater than 16 h) immersion in 50 mM borate buffer (pH 8.50), and (c) aminolyzed DSP-based adlayer on gold after immersion in 500 mM ethylamine in 50 mM borate buffer (pH 8.50). All band intensities (counts per second - CPS) have been normalized to the Au $(4f)_{7/2}$ band. The residuals (not shown) from the deconvolution analysis for S(2p), C(1s), N(1s), and O(1s) are 1.2, 2.6, 1.8, and 2.2%, respectively.

Table 2. XPS Band Assignments and Positions for As-Prepared and Reacted DSP-Based Monolayers[20,34−37]

		band position (eV)[a]		
core level	assignment	as-prepared	after hydrolysis	after aminolysis
O(1s)	carbonyl oxygen	532.1	532.0	531.1
O(1s)	NHS ester oxygen	534.4		
C(1s)	methylene carbon[b]	284.6	284.5	284.5
C(1s)	methylene carbon next to carbonyl carbon	285.3	285.4	286.0
C(1s)	carbonyl carbon	288.7	288.6	287.5
$S(2p_{3/2})$	gold-bound thiolate	161.9	162.0	162.0
$S(2p_{1/2})$	gold-bound thiolate	163.1	163.3	163.2
N(1s)	succinimidyl nitrogen	401.6		
N(1s)	amide nitrogen			399.5

[a]The uncertainty in the band positions is ±0.1 eV in the S(2p) region and up to 0.4 eV in the O(1s), C(1s) and N(1s) regions. [b]Assigned to methylene groups but unable to distinguish between those in the alkyl chains and the NHS group.

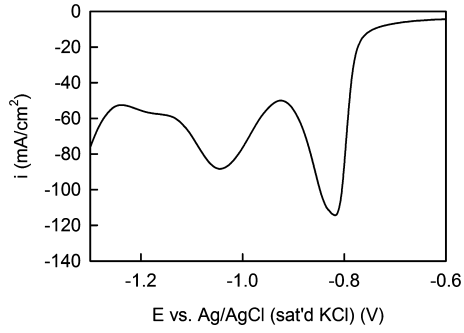

Figure 3. Linear voltammetric sweep (scan rate: 0.100 V/s) in 0.50 M KOH (aq) for the reductive desorption of the DSP-based adlayer on gold.

1265 cm^{-1}) follow this trend but are too weak in strength to be used for kinetic analysis.

The spectra in Figure 4 were analyzed to more fully characterize the hydrolysis kinetics by determining the temporal decrease in the strength of ν_a(C═O) of the adlayer. The bimolecular reaction rate for the base hydrolysis of the adlayer can be written as

$$\frac{d\Gamma_{NHS}}{dt} = -k_h\Gamma_{NHS}[OH^-] \quad (4)$$

where Γ_{NHS} is the surface concentration of the NHS reactive group (mol/cm^2), k_h is the second-order heterogeneous rate constant for hydrolysis (M^{-1} s^{-1}), [OH^-] is the hydroxide ion concentration in bulk solution (M), and t is time (s). Assuming that the conditions for a pseudo first-order reaction can be applied by use of a buffered alkaline solution, eq 4 can be simplified to

$$\frac{d\Gamma_{NHS}}{dt} = -k_h'\Gamma_{NHS} \quad (5)$$

dx.doi.org/10.1021/la503439g | Langmuir 2014, 30, 12868−12878

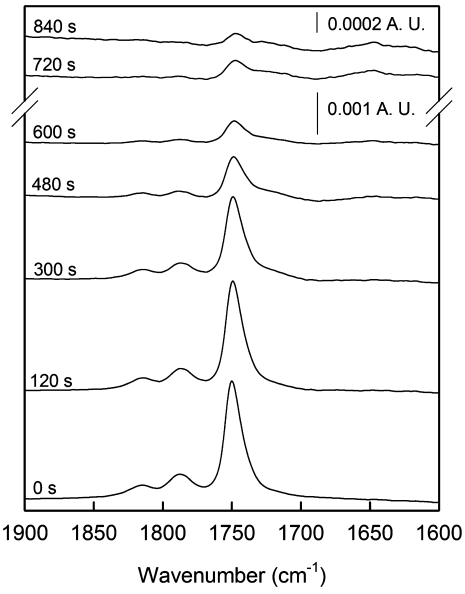

Figure 4. Infrared spectra of the DSP-based adlayer after different immersion times in 50 mM borate buffer (pH 8.50).

where k_h' is the pseudo first-order heterogeneous reaction rate constant (s^{-1}). Integration with the appropriate limits yields

$$\Gamma_{NHS(t)} = \Gamma_{NHS(t=0)} e^{-k_h' t} \quad (6)$$

The value of k_h' can be determined from the slope of a plot of $-\ln(1-x)$ vs t where x represents the extent of reaction, which is calculated from $(\Gamma_{NHS}(t)/\Gamma_{NHS}(t=0))$. This analysis assumes that Γ_{NHS} is directly proportional to the strength of ν_a(C═O) at 1748 cm^{-1}. Due to the so-called "infrared metal surface selection rule," this proportionality holds in IR-ERS only if the orientation of the transition dipole moment for this vibrational mode is constant throughout the reaction.[44] We have invoked this assumption in the analysis of these data.[45]

The results of this analysis are shown in Figure 5, which can be used to determine the time required for 50% conversion

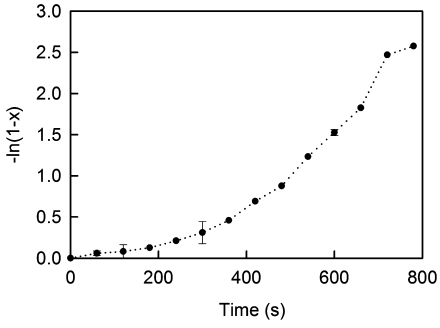

Figure 5. Kinetic plot for hydrolysis of the DSP-based monolayer in 50 mM borate buffer (pH 8.50). The dotted annotation between the experimental data points serve only as a guide to the eye. Some of the error bars are close to the size of the data point.

($t_{50\%}$) of 380 ± 40 s. In contrast to the linear relationship expected for a pseudo-first-order reaction, this plot has a nonlinear shape. There are a few possible interpretations for this dependence, including a difference in reaction order that can change with time and a reaction with two different rates that are connected in series. The former can be ruled out as the hydroxide ion is fixed by the use of 50 mM borate buffer (Experimental Section), which maintains the conditions of a pseudo first-order reaction. Thus, the shape of the kinetic plot is considered to originate from a progression of two reactions in series.

An interpretation of this type of rate profile, known as the Avrami or Johnson–Mehl–Avrami–Kolmogorov (JMAK) theorem, was originally proposed to describe the phase transitions in solids where a reaction at a surface can be divided into the three kinetic regimes depicted in Figure 6.[46−48] The three regimes are (1) a slow reaction rate at short times (t_1 and t_2) due primarily to the formation of reacting nuclei, i.e., the initiation stage; (2) a reaction interval at intermediate times (t_3 and t_4) with a more rapid and relatively constant rate in which previously formed nuclei grow in size and eventually form overlapping domains of reacted material, i.e., the bulk transformation stage; and (3) a period at long times (t_5) in which the rate slows as the reaction approaches completion. Indeed, the intermediate region (i.e., bulk transformation stage) in JMAK theory spans the extent of reaction from $0.15 < x < 0.8$, which corresponds to the time period from roughly 360 to 660 s in Figure 5.[49] We view the kinetic plot in Figure 5 to be comprised of three overlapping kinetic regimes, but with limited data to fully characterize the final regime due to a decrease in signal-to-noise such that the peak is no longer quantified with great certainty. In the initial stage (0 to ∼180 s), the reaction proceeds slowly, reflecting the role of a nucleation type of process in which the hydrolytic removal of NHS groups reduces steric barriers to the attack of hydroxide ions on the acyl carbon of esters at the edge of the nuclei. As time and the size of these growing domains increase (roughly 360 to 660 s), the rate of reaction undergoes an increase due to a greater number of accessible surface reactants. During this stage, the rate of the reaction becomes close to constant, which is indicative of an immeasurable change in the number of NHS groups at the domain boundaries. In the third and final regime (>720 s), the rate slows as the surface reactant is exhaustively consumed.

Based on the above interpretation, the reactivity of the adlayer was analyzed for our purposes via a pseudo first-order rate law in the bulk transformation stage. This analysis used a linear fit of the data between 360 and 660 s and gave a pseudo first-order reaction rate constant, k_h', of $4.6 \pm 0.3 \times 10^{-3}$ s^{-1}, and a second-order reaction rate constant, k_h, of $1.5 \pm 0.1 \times 10^3$ M^{-1} s^{-1} ($n = 3$). This value for k_h is much higher than that previously reported for this system in aqueous alkaline (1.00×10^{-3} M NaOH) solutions ($6.1 \pm 1.1 \times 10^{-1}$ M^{-1} s^{-1}).[50] While the origin(s) of the larger value found herein is presently unclear, we suspect that it reflects, at least in part, a difference in the number and/or size of structural defects in the adlayer, which is supported by wettability data.[35,51−53] For this adlayer system, Dordi et al. previously reported advancing (θ_a) and receding (θ_r) contact angles for water of 60 ± 2° and 39 ± 2°, respectively. We measured a comparable θ_a of 59 ± 2° ($n = 6$), but a much lower θ_r of 29 ± 5° ($n = 6$) which suggests that our adlayer is not as tightly packed as that in the earlier work. Experiments are now being designed to test for additional possible origins of this difference.

Homogeneous Base Hydrolysis. For comparative purposes, we measured the rates of the base hydrolysis for DSP and NBS (N-(benzoyloxy) succinimide) in aqueous solution. NBS served as a model for connection to the earlier work by Cline and Hanna which investigated the base hydrolysis of several types of NHS esters in both aprotic and aqueous

dx.doi.org/10.1021/la503439g | Langmuir 2014, 30, 12868−12878

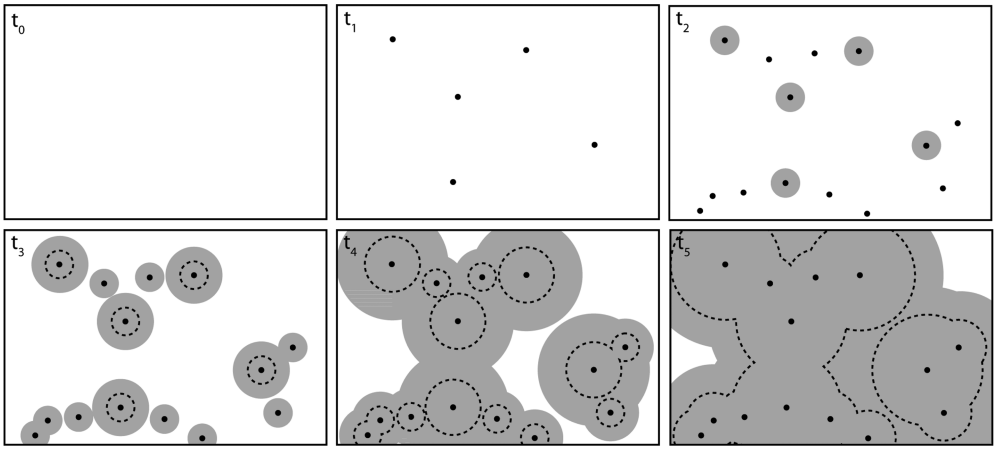

Figure 6. Schematic of an Avrami transformation from unreacted material at t_0 in which the rate is slow at small times (t_1 and t_2) due to the formation and initial growth of nuclei (black dots), i.e., the initiation stage; (2) more rapid at times t_3 and t_4 due to reacting nuclei (gray), i.e., the bulk transformation stage; and (3) low at long times (t_5) due to decreased amount of starting material (white). Dotted outlines show progression of reaction from t_3 to t_5.

solutions.[54] These UV-vis measurements monitored the reaction by following the appearance of the NHS anion with time. This anion adsorbs in the UV spectral region and has an absorbance maximum at 260 nm with a molar absorptivity of 9700 M^{-1} cm^{-1};[55] the neutral form of NHS absorbs much deeper in the UV region. By monitoring the reaction of NBS under the conditions used by Cline and Hanna (20% 1,4-dioxane and an ionic strength of 1.0 M through the addition of tetramethylammonium chloride, (TMAC)), we determined a second-order homogeneous reaction rate constant, $k_{h,solution}$ for NBS in 20% dioxane, of $9.2 \pm 0.7 \times 10^1$ M^{-1} s^{-1} ($n = 6$), which is in good agreement with the 8.7×10^1 M^{-1} s^{-1} value reported earlier.[54]

The reaction conditions used in subsequent experiments were analogous to those described previously for the interfacial experiments, borate buffer (50 mM, pH 8.50) with 1% 1,4-dioxane added for DSP solubility. Figure 7 shows the spectrophotometric data and the extent of reaction analysis for a 0.10 mM solution of DSP under these conditions. The absorbance initially increases rapidly, slowing to a limiting value as the reaction nears completion (~20 min). To quantify the reaction rate, the absorbance at 260 nm was monitored at 0.10 s increments. These data are shown in the inset of Figure 7. The plot exhibits the expected linear dependence for a pseudo first-order reaction. The analysis of this data gives a value of $k_{h,solution}$ for DSP of $8.6 \pm 0.5 \times 10^2$ M^{-1} s^{-1} ($n = 18$). For comparison, the value for $k_{h,solution}$ for NBS under these same conditions was $5.7 \pm 0.2 \times 10^2$ M^{-1} s^{-1} ($n = 9$); this reaction rate constant is larger than that reported earlier due to the inclusion of TMAC in that work, which is known to slow such reactions.[56]

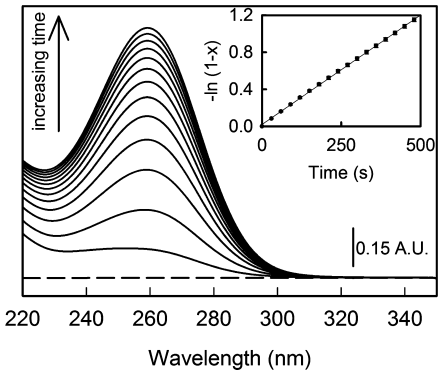

Figure 7. UV-vis absorption spectra for hydrolysis of 0.10 mM DSP in 50 mM borate buffer (pH 8.50) and 1% 1,4-dioxane. The spectrum of the blank (dotted line) is that for the reaction mixture without DSP present, which has been self-normalized. The first spectrum of the reaction mixture was obtained after mixing the reaction solution and collecting a spectrum, a time span of ~25 s. All subsequent spectra are displayed at intervals of ~100 s from the start of reaction. The inset is a pseudo first-order kinetic plot for the hydrolysis reaction based on solution absorbance at 260 nm. Some of the error bars are close to the size of the data point.

Previous studies have shown that the rates for the heterogeneous base hydrolysis of DSP-based monolayers and several other NHS esters are markedly retarded (100 to 1000x) in comparison to those found for the analogous homogeneous reactions.[50,57,58] In our case, however, the heterogeneous rate constant, k_h, for the DSP-based adlayer is nearly twice that of the value found in bulk solution. This finding indicates that the interfacial effects (i.e., sterics, polarity, etc.) often considered as slowing interfacial reaction rates do not play a significant role in the data reported in Figure 4.

Adlayer Aminolysis. For aminolysis reactivity studies, this investigation used ethylamine as a small molecule mimic of the amines in the lysine residues of immunoglobulin (IgG) proteins. Proteins like IgG can contain between 80 to 90 lysines per molecule,[59,60] and those located at the periphery of the protein structure have acid strengths (pK_a ~10.3)[61] similar to ethylamine (pK_a ~10.8).[62] The IR-ERS spectra for the temporal evolution of the reaction of the adlayer with 500 mM ethylamine (50 mM borate buffer, pH 8.50) are consistent with amide formation. Initially, there is a rapid decrease of the ν_a(C═O) for NHS at 1748 cm^{-1}, which at longer times is accompanied by the appearance of much weaker bands at 1665, 1556, and 1265 cm^{-1} (Figure 8 and Table 3) that can be assigned to amide I, amide II, and amide III vibrational modes, respectively.[63−65] Interestingly, the strength of ν_a(C═O) decreases by ~50% in 120 ± 30 s ($t_{50\%}$) ($n = 3$), whereas the same decrease for immersion in borate buffer only (Figure 4) required nearly 400 s. The more rapid loss of the NHS group reflects contributions from both the base hydrolysis and aminolysis reactions.

dx.doi.org/10.1021/la503439g | Langmuir 2014, 30, 12868−12878

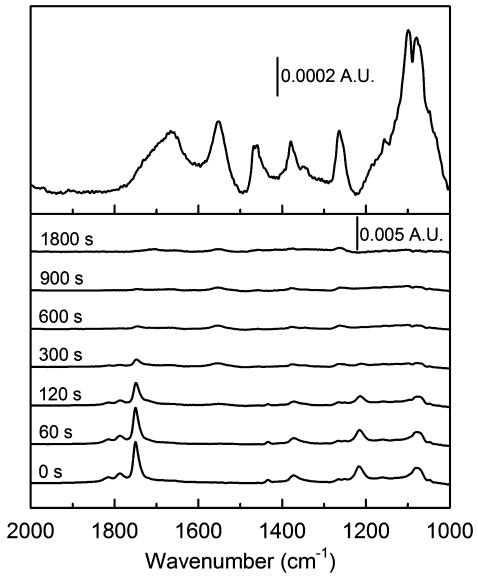

Figure 8. Infrared spectra of the DSP-based monolayer after immersion in 500 mM ethylamine in 50 mM borate buffer (pH 8.50) for 24 h (top) and various time steps (bottom).

The kinetic plot for the data in Figure 8 is shown in Figure 9. Due to the weakness of amide bands, this analysis tracked the decrease in the NHS carbonyl mode at 1748 cm^{-1}. To obtain the heterogeneous aminolysis reaction rate constant, the combined second-order rate laws for the two reactions occurring in parallel can be written as

$$\frac{d\Gamma_{NHS}}{dt} = -k_h\Gamma_{NHS}[OH^-] - k_a\Gamma_{NHS}[NH_2] \quad (7)$$

where k_a is the second-order heterogeneous rate constant for aminolysis (M^{-1} s^{-1}) and $[NH_2]$ is the deprotonated amine concentration in bulk solution (M). The corresponding integrated rate law is given by eq 8:

$$\Gamma_{NHS(t)} = \Gamma_{NHS(t=0)}e^{-(k_h[OH^-]+k_a[NH_2])t} \quad (8)$$

For comparative purposes, we analyzed the plot in Figure 9 at the time interval from 60 to 300 s, with the assumption that the rate in this time interval is representative of the bulk transformation stage for the two competing reactions per Avrami analysis. Thus, the time interval of 60 to 300 s yields a k_a of 9.4 ± 2.8 × 10^{-1} M^{-1} s^{-1}. In comparison, analyses using different time intervals in Figure 9 (0 to 600 s, 0 to 300 s, or 120 to 300 s) yielded k_a values of 0.09, 6.9, and 7.7 × 10^{-1} M^{-1} s^{-1}, respectively. These values differ at most by an order of magnitude in comparison to that for the 60 to 300 s interval. Hence, the analysis in the time interval of 60 to 300 s, which yields the largest value for k_a (i.e., the best case scenario for the effectiveness of the aminolysis reaction), can be used for a generalized comparison with the rate to hydrolysis.

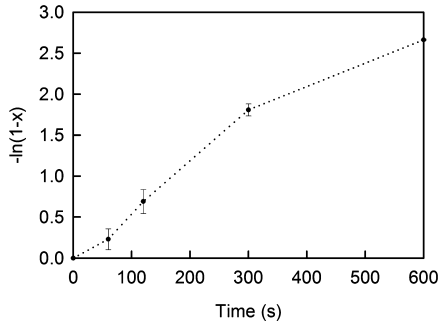

Figure 9. Kinetic plot for aminolysis of the DSP-derived adlayer in 500 mM ethylamine in 50 mM borate buffer (pH 8.50).

Implications of the Kinetic Measurements on the Aminolytic Immobilization of Proteins. The two reaction rate experiments show that the base hydrolysis reaction (k_h = 1.5 ± 0.1 × 10^3 M^{-1} s^{-1}) is inherently much faster than the aminolysis reaction (k_h = 9.4 ± 2.8 × 10^3 M^{-1} s^{-1}) at the DSP-based adlayer. To qualitatively estimate the impact of this difference, the relative rates of the two processes in the bulk transformation stage can be compared using the ratio, $r_{a/h}$, expressed as

$$\begin{aligned} r_{a/h} &= \frac{\nu_a}{\nu_h} \\ &= \frac{k_a\Gamma_{NHS}[NH_2]}{k_h\Gamma_{NHS}[OH^-]} \\ &= \frac{9.4\times10^{-1}[NH_2]}{1.5\times10^{3}[OH^-]} \\ &= 6.3\times10^{-4}\frac{[NH_2]}{[OH^-]} \end{aligned} \quad (9)$$

where ν_a is the reaction rate of aminolysis and ν_h is the reaction rate of hydrolysis. Equation 9 clearly points to the dominance of the base hydrolysis reaction in borate buffer (pH 8.50, 50 mM).

Per step 2 in Scheme 1, we typically use 100 μg/mL of antibody for immobilization,[66−68] which for IgG proteins (150 kDa) translates to ∼0.7 μM. Using this value for the amine concentration in eq 9, $r_{a/h}$ then equals 1.4 × 10^{-4}. In this case, the removal of the NHS terminal groups is completed (i.e., 99.9% conversion) in ∼210 s; however, less than 0.02% of the conversion is due to aminolysis. We can extend this projection by recognizing that the number of lysines sterically accessible at the periphery of an IgG protein ranges from 10 to 26.[59,60] If, neglecting the role of pH and the concomitant acceleration of the rate of base hydrolysis, we increase the apparent amine

Table 3. Infrared Spectral Peak Positions and Band Assignments for Aminolysis Reaction Products of the DSP-Based Monolayer[63−65]

mode assignment	mode description	peak position (cm^{-1})
ν_s(C═O)	free carboxylic acid	1742
80% ν(C═O)	amide I	1665
60% δ(N−H), 40% ν(C−N)	amide II	1556
$\delta(CH_2)$	methylene scissors deformation	1456
40% ν(C−N), 30% δ(N−H), 20% $\nu(CH_3-C)$	amide III	1265
ν_{as}(C−C,C−N)	CN, CC of $NHCH_2CH_3$	1107

dx.doi.org/10.1021/la503439g | Langmuir 2014, 30, 12868−12878

concentration by 26, $r_{a/h}$ increases to 3.6×10^{-3}, and the conversion of Γ_{NHS} due to aminolysis, while increasing to ~0.4%, remains insignificant. Moreover, we have yet to take into account the deprotonation state of the accessible amine groups. At a solution pH of 8.50, less than 2% of the sterically accessible amines are deprotonated, which works against improvements in the effectiveness of aminolysis (i.e., $r_{a/h}$ decreases to 5.6×10^{-5} and the conversion due to aminolysis drops below 0.01%).

In projecting the implications of eq 9 further, one could ask "what reactive amine concentration would be needed in order to make an argument in favor of protein tethering via aminolysis?" If, for example, the goal would be to achieve a value of $r_{a/h}$ of unity, the reactive amine (deprotonated) concentration would need to approach 5 mM. This concentration translates to an IgG protein level, assuming that 2% of the 26 sterically accessible amides are deprotonated at pH 8.50, of ~50 g/mL, which is, of course, not feasible. In other words, these kinetic data lead to the conclusion that the mechanism for protein coupling under the conditions in Scheme 1 has a minimal contribution (if any) to the formation of a layer of capture antibodies and that another pathway, i.e., adsorption, dominates the preparation process.

CONCLUSIONS

This work has endeavored to shed light on the use of NHS-ester monolayers in the immobilization of proteins, such as capture antibodies, in biosensor systems through IR-ERS reactivity studies of the desired aminolysis and competing hydrolysis reactions under common immunoassay conditions (borate buffer, pH 8.50). In contrast to the expected pseudo first-order linear reaction rate, the competing reaction of hydrolysis at the DSP-based monolayer surface gave evidence for a reaction in series with multiple reaction rates. An extension of JMAK theory was applied to describe these multiple kinetic regimes: an initiation stage with formation of reacting nuclei; a bulk transformation stage with rapid growth of the nuclei; and a final stage with slow growth. Applying an interpretation based on JMAK theory to the kinetic plots resulted in a tremendous difference in reaction rates for the competing hydrolysis and the desired aminolysis reactions. Moreover, these large differences in reaction rate constants clearly show that hydrolysis is the dominant reaction under conditions in which coupling agents are immersed in low protein concentrations and buffers of near physiological pH. Thus, this kinetic data points to the case in which the vast majority of the proteins immobilized per Scheme 1 are present due to electrostatic, hydrogen bonding, and van der Waals interactions, rather than by covalent linkages. There are a large number of diagnostic test platforms used in today's healthcare system that employ NHS-based chemistry for protein immobilization. The data herein suggests the possibility that adsorption may play a more important role in such processes than originally thought and that a reexamination of the immobilization chemistry may, in some cases, improve metrics of performance (e.g., reproducibility, limits of detection, etc.). To this end, future work will investigate the competing reactions of hydrolysis and aminolysis in NHS-based chemistries under various reaction conditions with the anticipation that further understanding of these competing reactions will help elucidate a means to achieve covalent coupling of proteins. These experiments will be reported elsewhere.

AUTHOR INFORMATION

Corresponding Author

*E-mail: marc.porter@utah.edu.

Notes

The authors declare no competing financial interest.

ACKNOWLEDGMENTS

This work was supported by the National Science Foundation Integrative Graduate Education Research Traineeship (IGERT NSF DGE-0903715), the National Institutes of Health (U01CA151650 and R33CA155586), and the Utah Science Technology and Research Initiative (USTAR). The XPS data in this paper was collected in the Utah Nanofab at the University of Utah, for which the authors thank Dr. Brian van Devener.

REFERENCES

(1) Jonkheijm, P.; Wieinrich, D.; Schroder, H.; Niemeyer, C. M.; Waldmann, H. Chemical Strategies for Generating Protein Biochips. *Angew. Chem., Int. Ed.* **2008**, *47*, 9618−9647.

(2) Rusmini, F.; Zhong, Z.; Feijen, J. Protein Immobilization Strategies for Protein Biochips. *Biomacromolecules* **2007**, *8*, 1775−1789.

(3) Hermansen, G. T. *Bioconjugate Techniques*, 2nd ed.; Academic Press, Inc.: New York, 2008.

(4) Patel, N.; Davies, M. C.; Hartshorne, M.; Heaton, R. J.; Roberts, C. J.; Tendler, S. J. B.; Williams, P. M. Immobilization of Protein Molecules onto Homogeneous and Mixed Carboxylate-Terminated Self-Assembled Monolayers. *Langmuir* **1997**, *13*, 6485−6490.

(5) Wagner, P.; Hegner, M.; Kernen, P.; Zaugg, F.; Semenza, G. Covalent Immobilization of Native Biomolecules onto Au(111) via *N*-Hydroxysuccinimide Ester Functionalized Self-Assembled Monolayers for Scanning Probe Microscopy. *Biophys. J.* **1996**, *70*, 2052−2066.

(6) Porter, M. D.; Lipert, R. J.; Siperko, L. M.; Wang, G.; Narayanan, R. SERS as a bioassay platform: fundamentals, design, and applications. *Chem. Soc. Rev.* **2008**, *37*, 1001−1011.

(7) Dufek, E. J.; Ehlert, B.; Granger, M. C.; Sandrock, T. M.; Legge, S. L.; Herrmann, M. G.; Meikle, A. W.; Porter, M. D. Competitive surface-enhanced Raman scattering assay for the 1,25-dihydroxy metabolite of vitamin D_3. *Analyst* **2010**, *135*, 2811−2817.

(8) Lomant, A. J.; Fairbanks, G. Chemical probes of extended biological structures: Synthesis and properties of the cleavable protein cross-linking reagent [^{35}S]dithiobis(succinimidyl propionate). *J. Mol. Biol.* **1976**, *104*, 243−261.

(9) Nuzzo, R. G.; Allara, D. L. Adsorption of Bifunctional Organic Disulfides on Gold Surfaces. *J. Am. Chem. Soc.* **1983**, *105*, 4481−4483.

(10) Xu, H.; Lu, J. R.; Williams, D. E. Effect of Surface Packing Density of Interfacially Adsorbed Monoclonal Antibody on the Binding of Hormonal Antigen Human Chorionic Gonadotrophin. *J. Phys. Chem. B* **2006**, *110*, 1907−1914.

(11) Madler, S.; Bich, C.; Touboul, D.; Zenobi, R. Chemical cross-linking with NHS esters: a systematic study on amino acid reactivities. *J. Mass. Spectrom.* **2009**, *44*, 694−706.

(12) Arakawa, T.; Timasheff, S. N. Preferential Interactions of Proteins with Salts in Concentrated Solutions. *Biochemistry* **1982**, *21*, 6545−6552.

(13) Chi, E. Y.; Krishnan, S.; Randolph, T. W.; Carpenter, J. F. Physical stability of proteins in aqueous solution: mechanism and driving forces in nonnative protein aggregation. *Pharm. Res.* **2003**, *20*, 1325−1336.

(14) Anjaneyulu, P. S. R.; Staros, J. V. Reactions of *N*-hydroxysulfosuccinimide active esters. *Int. J. Pept. Protein Res.* **1987**, *30*, 117−124.

(15) Grubor, N. M.; Shinar, R.; Jankowiak, R.; Porter, M. D.; Small, G. J. Novel biosensor chip for simultaneous detection of DNA-carcinogen adducts with low-temperature fluorescence. *Biosens. Bioelectron.* **2004**, *19*, 547−556.

(16) Wang, Q.; Kromka, A.; Houdkova, J.; Babchenko, O.; Rezek, B.; Li, M.; Boukherroub, R.; Szunerits, S. Nanomolar Hydrogen Peroxide Detection Using Horseradish Peroxidase Covalently Linked to Undoped Nanocrystalline Diamond Surfaces. *Langmuir* **2012**, *28*, 587−592.
(17) Darder, M.; Takada, K.; Pariente, F.; Lorenzo, E.; Abruna, H. D. Dithiobissuccinimidyl Propionate as an Anchor for Assembling Peroxidases at Electrodes Surfaces and Its Application in a H_2O_2 Biosensor. *Anal. Chem.* **1999**, *71*, 5530−5537.
(18) Cabrita, J. F.; Abrantes, L. M.; Viana, A. S. *N*-Hydroxysuccinimide-terminated self-assembled monolayers on gold for biomolecules immobilisation. *Electrochim. Acta* **2005**, *50*, 2117−2124.
(19) Veiseh, M.; Zareie, M. H.; Zhang, M. Highly Selective Protein Patterning on Gold-Silicon Substrates for Biosensor Applications. *Langmuir* **2002**, *18*, 6671−6678.
(20) Jiang, L.; Glidle, A.; Griffith, A.; McNeil, C. J.; Cooper, J. M. Characterising the formation of a bioelectrochemical interface at a self-assembled monolayer using X-ray photoelectron spectroscopy. *Bioelectrochem. Bioenerg.* **1997**, *42*, 15−23.
(21) Grdadolnik, J.; Marechal, Y. Bovine Serum Albumin Observed by Infrared Spectrometry. I. Methodology, Strutural Investigation, and Water Uptake. *Biopolymers* **2000**, *62*, 40−53.
(22) Frey, B. L.; Corn, R. M. Covalent Attachment and Derivatization of Poly(L-lysine) Monolayers on Gold Surfaces As Characterized by Polarization-Modulation FT-IR Spectroscopy. *Anal. Chem.* **1996**, *68*, 3187−3193.
(23) Dordi, B.; Pickering, J. P.; Schonherr, H.; Vancso, G. J. Probing chemical reactions on the nanometer scale: Inverted chemical force microscopy of reactive self-assembled monolayers. *Surf. Sci.* **2004**, *570*, 57−66.
(24) Norde, W.; MacRitchie, F.; Nowicka, G.; Lyklema, J. Protein adsorption at solid-liquid interfaces: Reversibility and conformation aspects. *J. Colloid Interface Sci.* **1986**, *112*, 447−156.
(25) Seah, M. P.; Smith, G. C.; Anthony, M. T. AES: Energy calibration of electron spectrometers. I-an absolute, traceable energy calibration and the provision of atomic reference line energies. *Surf. Interface Anal.* **1990**, *15*, 293−308.
(26) Shirley, D. A. High-Resolution X-Ray Photoemission Spectrum of the Valence Bands of Gold. *Phys. Rev. B* **1972**, *5*, 4709−4714.
(27) Moulder, J. F. *Handbook of X-ray Photoelectron Spectroscopy*. Physical Electronics, Inc.: Eden Prairie, MN, 1992.
(28) Walczak, M. M.; Popenoe, D. D.; Deinhammer, R. S.; Lamp, B. D.; Chung, C.; Porter, M. D. Reductive Desorption of Alkanethiolate Monolayers at Gold: A Measure of Surface Coverage. *Langmuir* **1991**, *7*, 2687−2693.
(29) Angerstein-Kozlowska, H. A.; Conway, B. E.; Hamelin, A.; Stoicoviu, L. Elementary steps of electrochemical oxidation of single-crystal planes of Au Part II. A chemical and structural basis of oxidation of the (111) plane. *J. Electroanal. Chem. Interfacial Electrochem.* **1987**, *228*, 429−453.
(30) Petrovykh, D. Y.; Kimura-Suda, H.; Whitman, L. J.; Tarlov, M. J. Quantitative Analysis and Characterization of DNA Immobilized on Gold. *J. Am. Chem. Soc.* **2003**, *125*, 5219−5226.
(31) Petrovykh, D. Y.; Kimura-Suda, H.; Tarlov, M. J.; Whitman, L. J. Quantitative Characterization of DNA Films by X-ray Photoelectron Spectroscopy. *Langmuir* **2004**, *20*, 429−440.
(32) Powell, C. J.; A, J. *NIST Electron Effective-Attenuation-Length Database*, Version 1.0 (SRD-82); U.S. Department of Commerce, National Institute of Standards and Technology: Gaithersburg, MD, 2001.
(33) McKittrick, P. T.; Katon, J. E. Infrared and Raman Group Frequencies of Cyclic Imides. *Appl. Spectrosc.* **1990**, *44*, 812−817.
(34) Delamarche, E.; Sundarababu, G.; Biebuyck, H.; Michel, B.; Gerber, C.; Sigrist, H.; Wolf, H.; Ringsdorf, H.; Xanthopoulos, N.; Mathieu, H. J. Immobilization of Antibodies on a Photoactive Self-Assembled Monolayer on Gold. *Langmuir* **1996**, *12*, 1997−2006.
(35) Bain, C. D.; Troughton, E. B.; Tao, Y. T.; Evall, J.; Whitesides, G. M.; Nuzzo, R. G. Formation of Monolayer Films by the Spontaneous Assembly of Organic Thiols from Solution onto Gold. *J. Am. Chem. Soc.* **1989**, *111*, 321−335.
(36) Bain, C. D.; Biebuyck, H. A.; Whitesides, G. M. Comparison of Self-Assembled Monolayers on Gold: Coadsorption of Thiols and Disulfides. *Langmuir* **1989**, *5*, 723−727.
(37) Cho, Y.; Ivanisevic, A. TAT Peptide Immobilization on Gold Surfaces: A Comparison Study with a Thiolated Peptide and Alkylthiols Using AFM, XPS, and FT-IRRAS. *J. Phys. Chem. B* **2005**, *109*, 6225−6232.
(38) Laredo, T.; Leitch, J.; Chen, M.; Burgess, I. J.; Dutcher, J. R.; Lipkowski, J. Measurement of the Charge Number Per Adsorbed Molecule and Packing Densities of Self-Assembled Long-Chain Monolayers of Thiols. *Langmuir* **2007**, *23*, 6205−6211.
(39) Schneider, T. W.; Buttry, D. A. Electrochemical Quartz Crystal Microbalance Studies of Adsorption and Desorption of Self-Assembled Monolayers of Alkyl Thiols on Gold. *J. Am. Chem. Soc.* **1993**, *115*, 12391−12397.
(40) Yang, D. F.; Wilde, C. P.; Morin, M. Studies of the Electrochemical Removal and Efficient Re-formation of a Monolayer of Hexadecanethiol Self-Assembled at an Au(111) Single Crystal in Aqueous Solutions. *Langmuir* **1997**, *13*, 243−249.
(41) Zhong, C. J.; Zak, J.; Porter, M. D. Voltammetric reductive desorption characteristics of alkanethiolate monolayers at single crystal Au(111) and (110) electrode surfaces. *J. Electroanal. Chem.* **1997**, *421*, 9−13.
(42) Porter, M. D.; Bright, T. B.; Allara, D. L.; Chidsey, C. E. D. Spontaneously Organized Molecular Assemblies. 4. Structural Characterization of *n*-Alkyl Thiol Monolayers on Gold by Optical Ellipsometry, Infrared Spectroscopy, and Electrochemistry. *J. Am. Chem. Soc.* **1987**, *109*, 3559−3568.
(43) Nuzzo, R. G.; Fusco, F. A.; Allara, D. L. Spontaneously Organized Molecular Assemblies. 3. Preparation and Properties of Solution Adsorbed Monolayers of Organic Disulfides on Gold Surfaces. *J. Am. Chem. Soc.* **1987**, *109*, 2358−2368.
(44) Porter, M. D. IR External Reflection Spectroscopy: A Probe for Chemically Modified Surfaces. *Anal. Chem.* **1988**, *60*, 1143A−1155A.
(45) We view this assumption as reasonable since there is not detectable change in the absolute strengths of C−H the stretching modes between 2800 and 3000 cm^{-1} (data not shown).
(46) Avrami, M. Kinetics of Phase Change. II Transformation-Time Relations for Random Distribution of Nuclei. *J. Chem. Phys.* **1940**, *8*, 212−224.
(47) Avrami, M. Granulation, Phase Change, and Microstructure Kinetics of Phase Change. III. *J. Chem. Phys.* **1941**, *9*, 177−184.
(48) Vinokurov, I. A.; Morin, M.; Kankare, J. Mechanism of Reductive Desorption of Self-Assembled Monolayers on the Basis of Avrami Theorem and Diffusion. *J. Phys. Chem. B* **2000**, *104*, 5790−5796.
(49) Fatemi, N.; Whitehead, R.; Price, D.; Dollimore, D. Some Comments on the Use of Avrami-Erofeev Expressions and Solid State Decomposition Rate Constants. *Thermochim. Acta* **1986**, *104*, 93−100.
(50) Dordi, B.; Schonherr, H.; Vancso, G. J. Reactivity in the Confinement of Self-Assembled Monolayers: Chain Length Effects on the Hydrolysis of *N*-Hydroxysuccinimide Ester Disulfides on Gold. *Langmuir* **2003**, *19*, 5780−5786.
(51) Ulman, A. Formation and structure of self-assembled monolayers. *Chem. Rev.* **1996**, *96*, 1533−1554.
(52) Schonherr, H.; Chechik, V.; Stirling, C. J. M.; Vancso, G. J. Monitoring Surface Reactions at an AFM Tip: An Approach To Follow Reaction Kinetics in Self-Assembled Monolayers on the Nanometer Scale. *J. Am. Chem. Soc.* **2000**, *122*, 3679−3687.
(53) A rigorous analysis of the reaction rate for the base hydrolysis of esters includes an accounting of the reaction with H_2O. We did not detect any conversion for the homogeneous and heterogeneous reactions of DSP in water after 24 h.
(54) Cline, G. W.; Hanna, S. B. Kinetics and mechanisms of the aminolysis of *N*-Hydroxysuccinimide esters in aqueous buffers. *J. Org. Chem.* **1988**, *53*, 3583−3586.

(55) Miron, T.; Wilchek, M. A Spectrophotometric Assay for Soluble and Immobilized *N*-Hydroxysuccinimide Esters. *Anal. Biochem.* **1982**, *126*, 433−435.
(56) Baltzly, R.; Berger, I. M.; Rothstein, A. A. The Aminolysis of Esters. A Preliminary Study. *J. Am. Chem. Soc.* **1950**, *72*, 4149−4152.
(57) Chechik, V.; Stirling, C. J. M. Reactivity in Monolayers versus Bulk Media: Intra- and Intermolecular Aminolysis of Esters. *Langmuir* **1997**, *13*, 6354−6356.
(58) Chechik, V.; Crooks, R. M.; Stirling, C. J. M. Reactions and Reactivity in Self-Assembled Monolayers. *Adv. Mater.* **2000**, *12*, 1161−1171.
(59) Southwick, P. L.; Ernst, L. A.; Tauriello, E. W.; Parker, S. R.; Mujumdar, R. B.; Mujumdar, S. R.; Clever, H. A.; Waggoner, A. S. Cyanine Dye Labeling Reagents - Carboxymethylindocyanine Succinimidyl Esters. *Cytometry* **1990**, *11*, 418−430.
(60) Nakagawa, Y.; Capetillo, S.; Jirgensons, B. Effect of Chemical Modifcation of Lysine Residues on the Conformation of Human Immunoglobulin G. *J. Biol. Chem.* **1972**, *247*, 5703−5708.
(61) Zhang, M.; Vogel, H. J. Determination of the Side Chain pK_a Values of the Lysine Residues in Calmodulin. *J. Biol. Chem.* **1993**, *268*, 22420−22428.
(62) Lyde, D. R. *CRC Handbook of Chemistry and Physics 2004-2005: A Ready-Reference Book of Chemical and Physical Data*; CRC Press: Boca Raton, FL, 2004.
(63) Miyazawa, T.; Shimanouchi, T.; Mizushima, S. I. Characteristic Infrared Bands of Monosubstituted Amides. *J. Chem. Phys.* **1956**, *24*, 408−418.
(64) Miyazawa, T.; Shimanouchi, T.; Mizushima, S. I. Normal Vibrations of *N*-Methylacetamide. *J. Chem. Phys.* **1958**, *29*, 611−616.
(65) Zeroka, D.; Jensen, J. O.; Samuels, A. C. Infrared spectra of some isotopomers of ethylamine and the ethylammonium ion: a theoretical study. *J. Mol. Struct.* **1999**, *465*, 119−139.
(66) Driskell, J. D.; Kwarta, K. M.; Lipert, R. J.; Porter, M. D.; Neill, J. D.; Ridpath, J. F. Low-Level Detection of Viral Pathogens by a Surface-Enhanced Raman Scattering Based Immunoassay. *Anal. Chem.* **2005**, *77*, 6147−6154.
(67) Grubisha, D. S.; Lipert, R. J.; Park, H. Y.; Driskell, J.; Porter, M. D. Femtomolar Detection of Prostate-Specific Antigen: An Immunoassay Based on Surface-Enhanced Raman Scattering and Immunogold Labels. *Anal. Chem.* **2003**, *74*, 5936−5945.
(68) Yakes, B. J.; Lipert, R. J.; Bannantine, J. P.; Porter, M. D. Detection of *Mycobacterium avium* subsp. *paratuberculosis* by a Sonicate Immunoassay Based on Surface-Enhanced Raman Scattering. *Clin. Vaccine Immunol.* **2008**, *15*, 227−234.